Eur. Phys. J. A **31**, 185–194 (2007)
DOI 10.1140/epja/i2006-10166-9

THE EUROPEAN PHYSICAL JOURNAL A

Regular Article – Nuclear Structure and Reactions

Excitation functions of fusion reactions and neutron transfer in the interaction of ^{6}He with ^{197}Au and ^{206}Pb

Yu.E. Penionzhkevich[1], R.A. Astabatyan[1], N.A. Demekhina[2], G.G. Gulbekian[1], R. Kalpakchieva[1], A.A. Kulko[1,a], S.M. Lukyanov[1], E.R. Markaryan[1], V.A. Maslov[1], Yu.A. Muzychka[1], Yu.Ts. Oganessian[1], R.V. Revenko[1], N.K. Skobelev[1], Yu.G. Sobolev[1], D.A.Testov[1], and T. Zholdybaev[3]

[1] Joint Institute for Nuclear Research, 141980 Dubna, Russia
[2] Yerevan Physics Institute, Yerevan, Armenia
[3] Institute of Nuclear Physics, Almaty-82, Kazakhstan

Received: 13 June 2006 / Revised: 7 December 2006
Published online: 25 January 2007 –
Communicated by D. Guerreau

Abstract. Excitation functions for evaporation residues in the reactions ^{197}Au(^{6}He, xn)$^{203-x\mathrm{n}}$Tl, $x = 2$–7, and ^{206}Pb(^{6}He, 2n)^{210}Po, as well as for neutron transfer reactions for the production of ^{196}Au and ^{198}Au in the interaction of ^{6}He with ^{197}Au were measured. The ^{6}He beam was obtained from the accelerator complex for radioactive beams DRIBs (JINR). The maximum energy of the beam was about 10 AMeV and the intensity reached 2×10^{7} pps. The stacked-foil activation technique was used directly in the beam extracted from the cyclotron or in the focal plane of the magnetic spectrometer MSP-144. The identification of the reaction products was done by their radioactive γ- or α-decay. The fusion reaction with the evaporation of two neutrons was characterized by an increase in the cross-section compared to statistical model calculations. The analysis of the data in the framework of the statistical model for the decay of excited nuclei, which took into account the sequential fusion of ^{6}He has shown good agreement between the experimental and the calculated values of the cross-sections in the case of sub-Coulomb-barrier fusion in the ^{206}Pb + ^{6}He reaction. An unusually large cross-section was observed below the Coulomb barrier for the production of ^{198}Au in the interaction of ^{6}He with ^{197}Au. Possible mechanisms of formation and decay of transfer reaction products are discussed.

PACS. 25.60.-t Reactions induced by unstable nuclei – 25.60.Pj Fusion reactions – 25.60.Je Transfer reactions

1 Introduction

It has been found long ago that the fusion of stable nuclei at energies close to the Coulomb barrier strongly depends on the coupling with other reaction channels, in particular with direct reactions [1,2]. In the case of some light neutron-rich nuclei an extended distribution of nuclear matter is observed and the presence of valence neutrons can lead to the formation of a neutron halo, characterized by small separation energy of the constituent nucleons. ^{6}He is such an example. The reactions with halo nuclei have aroused much interest and continue to be a challenge both to experiment and theory. In particular, much effort has been devoted to studying near-barrier fusion of light weakly bound nuclei. What concerns the interaction of the neutron-rich halo nucleus ^{6}He with stable targets, one can expect increased fusion cross-section due to the reduction of the reaction Coulomb barrier because of the larger radius. On the other hand, the weak binding of the halo neutrons leads to a higher breakup probability of the nuclei which, in turn, reduces the fusion cross-section. Consequent capture of the residual nucleus (the core) by the target nucleus or transfer of nucleons without any further interaction between the nuclei can take place. The exchange of one or several nucleons between the target and projectile, inelastic scattering, etc. are also probable. However, if the couplings between fusion and transfer reactions with positive Q-value are taken into account, it is expected that the fusion involving ^{6}He will be enhanced [3] similarly to the cases observed for stable beams [1,2,4]. In any case, the variety of processes makes it difficult to analyze the experimental data and requires the consideration of all possible reaction channels.

Fusion and breakup reactions with halo nuclei have been studied by different groups. A detailed picture of the situation both from experimental and theoretical point of view can be found in the recently published reviews [5,6].

[a] e-mail: kulko@nrmail.jinr.ru

In an early experiment [7] with the radioactive ^{6}He beam the reaction ^{209}Bi + ^{6}He was used to measure the energy dependence of the cross-section for the 4n evaporation channel and for fission of the compound nucleus ^{215}At. It was claimed that an enhancement was observed at relatively low energies compared to similar results from ^{4}He-induced reactions and to theoretical expectations based on the one-dimensional barrier penetration model. Such an enhancement as a consequence of the increase of the probability of penetrating (tunneling) through the potential barrier due to the extended neutron distribution, compared to that in ordinary nuclei close to the line of stability, was predicted for halo nuclei in a series of theoretical papers; nevertheless, a satisfactory conclusion on the issue could not be made as the reduction of the probability for fusion at energies below the barrier was also anticipated [5,6].

Several subsequent experiments aimed to determine the probability of fusion of ^{6}He with other nuclei close to the Coulomb barrier have not been able to resolve this conflicting situation. Here are some examples. In [8], the excitation function for the decay of the compound nucleus by emission of three neutrons was measured using (as in [7]) the reaction ^{209}Bi + ^{6}He. The comparison with the statistical model for the formation and decay of the compound nucleus confirmed that an enhancement of the sub-barrier fusion of ^{6}He nuclei takes place. It was argued in [8] that the observed enhancement might result from coupling to positive Q-value neutron transfer channels, that leads to a reduction in the fusion barrier. Suppression of fusion due to projectile breakup was not observed. The following measurement of the excitation function for the fission channel in the ^{6}He + ^{238}U reaction [9] also allowed to conclude that the probability of fusion-fission with a ^{6}He beam at Coulomb barrier energies was strongly enhanced. However, an experiment of the same group involving the measurement of the fission fragments in coincidence with α-particles, produced after the breakup of ^{6}He, showed that the sub-barrier fusion-fission for this reaction could be explained in terms of the fission of the uranium target after the transfer of one or two neutrons. This circumstance led to a new paper [10] with the statement that no enhancement of the fusion of ^{6}He was present in the mentioned reaction. There are a few more papers reporting on ^{6}He-induced reactions, *e.g.* [11–14]. In [11], fusion excitation functions as well as angular distributions for the other open channels —elastic scattering, transfer and breakup— were measured at near-Coulomb-barrier energies and compared for the two reactions ^{6}He + ^{64}Zn and ^{4}He + ^{64}Zn. It was concluded that the transfer and breakup reaction mechanisms are predominant, whereas no enhancement of the fusion cross-section of ^{6}He was observed relative to that for ^{4}He. Instead of using inclusive α-particle measurements as in [11,13], in [12] inclusive in-beam γ-ray detection and coincidences between the heavy reaction products (identified by their characteristic γ-rays) and the projectile-like charged particles have been applied for the ^{6}He + ^{63,65}Cu reactions. In this experiment also, direct evidence was found for large transfer cross-sections compared to those obtained with a ^{4}He beam and to expectations from statistical model analysis; however, here the lowest used ^{6}He incident energy was 10 MeV higher than the reaction Coulomb barrier. Also recently, a neutron-α-particle coincidence experiment, aimed to separate the different reaction mechanisms responsible for α-particle emission, has shown a relatively strong contribution of one-neutron transfer in the ^{209}Bi + ^{6}He reaction [14]. This is in line with discussions in [13] of the increased two-neutron transfer observed in the same reaction.

However, conclusions from measurements of this type require the inclusion of more information on the different exit channels and higher statistics in order to be considerably more reliable. In spite of the increasing number of studies with different exotic nuclei, there is still controversy in the interpretation of the data obtained and the discussion about the effect of the halo structure on the reaction mechanism is still open.

The existence of such controversial data is the evidence of the difficulties which have to be overcome in experiments with radioactive ion beams. In the first place —this is the low intensity of the secondary beams. Hence, measurements in the region of the Coulomb barrier are extremely time consuming, if high statistics is to be obtained. Secondly, in order to study the excitation functions in a broad energy range (5–70 MeV), it is often necessary to decrease the beam energy using degraders, which in turn causes deterioration of the beam energy dispersion. Finally, at a relatively low beam intensity, it is desirable to use high-efficiency experimental techniques.

It seems that such conditions can be at present provided only at facilities based on the ISOL method. Such facilities, in addition to DRIBs, are SPIRAL1 in France and the accelerator at Louvain-la-Neuve (Belgium).

All this was taken into account when preparing the experiments described below. The launching of the Dubna accelerator complex for radioactive beams DRIBs [15] at FLNR (JINR) made it possible to produce ^{6}He beams with an intensity of up to 2×10^{7} pps. The maximum extracted energy was about 10 MeV/A, the energy resolution being not worse than 1–1.5%. The results of the first experiment studying the interaction of ^{6}He with the target nuclei ^{197}Au and ^{206}Pb have been already published in [16].

In the present paper we report on new measurements which were aimed at studying the interaction of ^{6}He with ^{197}Au and ^{206}Pb. The excitation functions of the fusion reactions with the consequent evaporation of 2 to 7 neutrons from the compound nuclei and of transfer reactions on ^{197}Au with the formation of ^{198}Au, ^{196}Au and ^{194}Au were measured. A beam dose about a factor of 10 higher than in [16] was used, and the energy range was extended to energies significantly lower than the Coulomb barrier of the reactions.

2 Experimental method

In the experiments a beam of accelerated ^{6}He ions with an energy of up to about 10 MeV/A was used. It was provided

Table 1. Summary of ^{6}He bombarding conditions related to the stacks: initial ^{6}He beam energy (E_{ini}), energy incident on first target (E_{1tar}), energy spread ΔE (FWHM) and beam intensity (I). $**$: present work.

Run No.	E_{ini} [MeV]	ΔE [MeV]	E_{1tar} [MeV]	ΔE [MeV]	I [pps]	Ref.
1.	60.3	±0.4	60.3 (Au) 21.8 (Pb)	±0.4	$5 \cdot 10^6$	[16]
2.	60.9	±0.4	43.3 (Au)	±0.6	$2 \cdot 10^6$	**
3.	61.2	±0.8	25.5 (Pb) 10.3 (Au)	±1.1 ±2.3	$\sim 10^7$	**
4.	61.9	±0.7	23.3 (Au)	±0.25	$5 \cdot 10^5$	**

by the DRIBs complex at FLNR, JINR [15]. This complex is a tandem including the FLNR cyclotrons U400M and U400. The ^{6}He nuclei were produced in a thick beryllium or carbon target bombarded with a ^{7}Li beam accelerated to 35 MeV/A (its intensity being $\sim 1.5\,\mathrm{e}\mu$A) at the U400M accelerator and diffused into the ECR source chamber from a porous carbon catcher (heated up to 1600 °C). After ionization of the ^{6}He atoms in the ion source, the single-charged ^{6}He ions were transported to the second accelerator U400, where they were further accelerated to an energy of about 10 MeV/A with intensity up to 2×10^7 pps. The ^{6}He^{+2} beam was extracted from the U400 cyclotron by a thin aluminum stripping foil. For beam diagnostics and tuning of the low-energy ^{6}He ions, scintillation detectors were placed [17] along the beam transport line. The optimization and transport of the ^{6}He^{+2}-ion beam made it possible, without applying any additional collimation, to have a (7×7) mm^2 beam spot on the physical targets. The beam profile and intensity were measured with a specially designed multi-wire proportional diagnostic chamber [18] situated immediately in front of the physical setup.

A total of four runs were carried out (see table 1). The energy of the extracted ^{6}He beam after passing through the diagnostic chamber is given in the second column. It was measured with the MSP-144 magnetic spectrometer [19] or with a semiconductor detector placed at 0° relative to the beam direction. The energies of the beam incident on the first gold or lead target in the stack (column 4) and their energy spread (column 5) were directly measured. The energies on the following targets were determined either by measurements inserting them one after the other into the stack, or by interpolation after measuring the energy incoming and exiting the stack. In the latter case, the error in determining these "average" values is due to the error in the target thickness and in the stopping power since different programmes give slightly different stopping power values. In any case, the energy values corresponding to each cross-section point in the measured excitation functions refer to the middle of the targets.

In all runs, the measurement of the yields of the fusion reaction evaporation residues and of the transfer reactions was performed by the stacked-foil activation technique. This method has the considerable advantage, particularly important for experiments with secondary beams, of allowing to obtain simultaneously in a single irradiation the cross-sections of a large amount of exit-channel products.

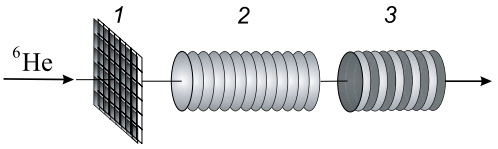

Fig. 1. Schematic layout of the activation experiments using the ^{6}He beam (Run 1): 1, multi-wire proportional chamber; 2, stack of gold foils and 3, stack of thin ^{206}Pb targets, as described in the text.

The details of Run 1 are presented in ref. [16]. Here we shall mention them only briefly. Two stacks of foils were placed in the reaction chamber of the magnetic spectrometer MSP-144 one after the other: first —a stack consisting of one 50 μm and twelve 13.5 μm thick gold foils, and further downstream —a second stack of six ^{206}Pb targets, 600–700 μg/cm^2 each on $\sim$ 1.5 μm Mylar backing, with 20 μm thick Al beam energy degraders in between the targets (fig. 1).

After passing through the two stacks, the beam entered the magnetic spectrometer MSP-144, which gave a precise measurement of the residual energy of the beam. The ^{6}He energy and the energy loss in each layer of the stacks were calculated with the LISE code [20] and the calculated residual energy was compared to the value measured by the magnetic spectrometer. In this way, in spite of the rather large energy spread of the beam after the last target (FWHM $\approx \pm3$ MeV), the absolute value of the energy at the center of each target was determined with good accuracy (better than 1 MeV).

In Run 2 only a stack of fifteen ^{197}Au (seven 13.5 μm, four 5 μm and four 4 μm) targets was irradiated. In order to reduce (compared to Run 1) the energy and angular straggling, and hence the energy spread at lower incident energies, different energy absorbers were employed to decrease the initial energy of the beam down to 43.3 MeV. In this run, the energy incident on each successive target (or the energy exiting the previous one) was determined separately (using the semiconductor monitor detector at 0°) step-by-step by inserting the targets into the stack one after another. The beam energy at each cross-section point was taken as the average of entrance and exit energies. The measured FWHM for each target was used to define the spread in the energy values for each cross-section point.

In Run 3, the initial energy of the extracted ^{6}He beam was lowered to 25.5 MeV by means of two foils: a gold one, which simultaneously served as a target for the excitation function on ^{197}Au, and an Al one. A stack of seven thin ^{206}Pb targets on Havar backings (also playing the role of energy degraders) was used. After it, two 5 μm ^{197}Au targets were placed in order to measure the transfer reactions deeply below ($E \leq 10$ MeV) the Coulomb barrier of the reaction ($B_c \approx 20.9$ MeV). As in Run 2, before the stack was finally assembled and irradiated, the energy of the beam incident on each successive target was measured by the monitor detector at 0°. In this case, since the energy loss

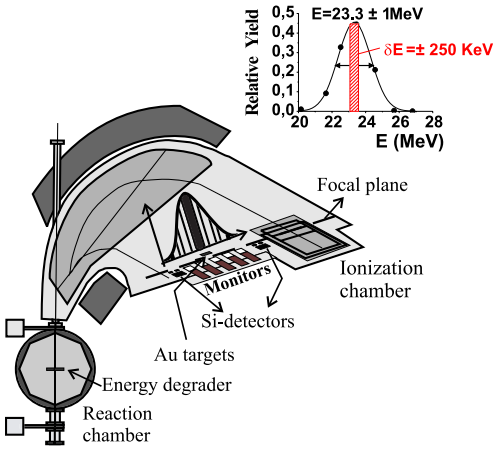

Fig. 2. (Colour online) Schematic layout of the activation experiments using the MSP-144 magnetic spectrometer. The inset presents the energy measurement at the focal plane.

in the Pb layers was very small, the measured value was used for the excitation function. During the irradiation, the monitor, with a calibrated mesh attenuator installed in front of it, was kept in the beam to control its stability.

In Run 4, the stringent requirements, concerning the stability of the beam and the necessity to reduce as much as possible the energy spread of the beam falling on the ^{197}Au targets at very low energies, were met by placing the stack of gold foils on the focal plane of the magnetic spectrometer MSP-144 [19]. The layout of the experimental setup is shown in fig. 2. The initial energy of the ^{6}He beam was reduced to 23.3 MeV and its value and spatial distribution were measured by varying the magnetic field in the magnetic spectrometer: two independent detection arrays were used —the MSP focal-plane detector and two PIN detectors placed at two different positions on the focal plane. After this, the new ^{197}Au target stack, consisting of 7 foils (each 6.6 μm thick), was placed at the position of the maximum beam intensity. In this case, the energy of the beam impinging on the stack was $E \pm \delta E$, where δE was determined by the extension (18 mm) of the target along the focal plane, which corresponded to a value of $\pm$250 keV (shown in the inset of fig. 2). The beam dose on the stack was measured by a scintillation counter behind it. On both sides, other counters were placed for additional control of the beam. The long-term high stability (about 10^{-5}) of the magnetic field of the spectrometer allowed defining the final energy spread for each calculated cross-section point mainly by the energy loss in each target.

After the irradiation, the γ-activity induced in the individual gold foils was measured off-line using four energy and efficiency-calibrated HPGe detectors (the efficiency was about 4–5% for $E_\gamma = 662$ keV) of high-energy resolution (1.2 keV for the γ-transition at 1332 keV). For the analysis of the γ-spectra, the program DEIMOS 32 [21] was used. Table 2 contains the decay data —energies, half-lives and absolute yields of the most intensive γ-transitions which have been used for the identification off-line of the corresponding reaction products. Peaks in the

Table 2. Characteristics of the decay products of the compound nucleus ^{203}Tl and of the ^{194}Au, ^{195}Au, ^{196}Au, ^{198}Au and ^{199}Au isotopes [22].

Decay product	Half-life $T_{1/2}$	E_γ, keV	I %
^{201}Tl	72.91 h	167.4	10
^{200}Tl	26.1 h	367.9	87
		579.3	13.8
		1205.7	29.9
^{199}Tl	7.42 h	247.3	9.3
^{198}Tl	5.3 h	675.9	11
^{198m}Tl	1.87 h	587.2	52
		282.8	28
^{197}Tl	2.84 h	152.2	7.3
^{196}Tl	1.84 h	344.9	2
^{196m}Tl	1.41 h	505.2	6
		695.6	41
^{194}Au	38.02 h	293.5	10.4
		328.4	61
^{195}Au	186.09 d	98.8	10.9
^{196g}Au	6.183 d	333	22.9
		355.7	86.9
^{196m2}Au	9.6 h	147.7	43
		188.2	37.4
^{198g}Au	2.696 d	411.8	95.5
^{198m}Au	2.3 d	180.3	50
		204.1	40.8
		214.9	77
^{199}Au	3.139 d	158.4	40
		208.2	8.7

measured γ-ray spectra (see, for example, fig. 3) could be identified as belonging to the Tl isotopes, which are the decay products of the compound nucleus ^{203}Tl after the evaporation of 2–7 neutrons. The production of the isotopes ^{194}Au, ^{196}Au and ^{198}Au was also observed, including at incident energies below 10 MeV, *e.g.* fig. 4.

The absolute cross-sections for the formation of the reaction products were calculated taking into account the relevant beam dose and time factors, the target thickness and the decay characteristics of the identified isotopes using the formula from [23]:

$$\sigma = \frac{S\ \lambda\ e^{\lambda t_2}}{\phi\ N_{at}\ \varepsilon\ I_\gamma\ (1-e^{-\lambda t_1})(1-e^{-\lambda t_3})},$$

where S is the number of counts in the photopeak for the time of γ-spectrum measurement t_3, λ —the decay constant of a given isotope, t_2 —the time elapsed between the end of irradiation and the start of the γ-activity measurement, t_1 —the time of irradiation, d —the target thickness in atoms/cm^2, ϕ —the beam intensity in unit time, I —the absolute intensity of the given γ-transition, and ϵ —the γ-detector efficiency for the given γ-line.

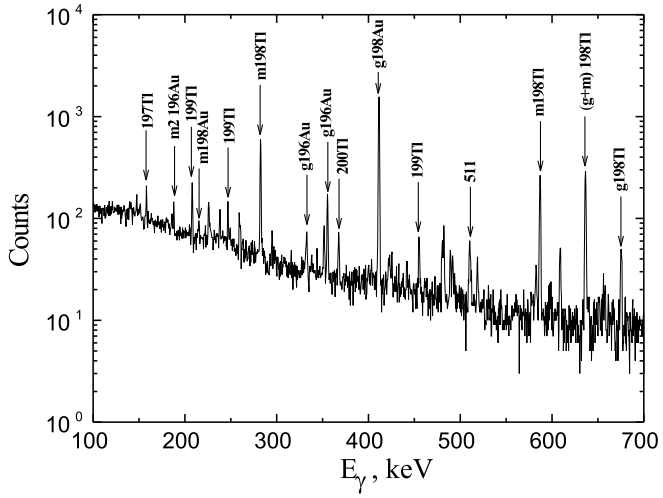

Fig. 3. Fragment of the γ-spectrum, obtained from measurement of the induced activity in the 13.5 μm Au-foil irradiated with the ^{6}He beam at $\sim$ 43 MeV (Run 2). The γ-transition identification is shown next to the peaks. The formation of the ground and isomeric states is denoted by g and m, respectively.

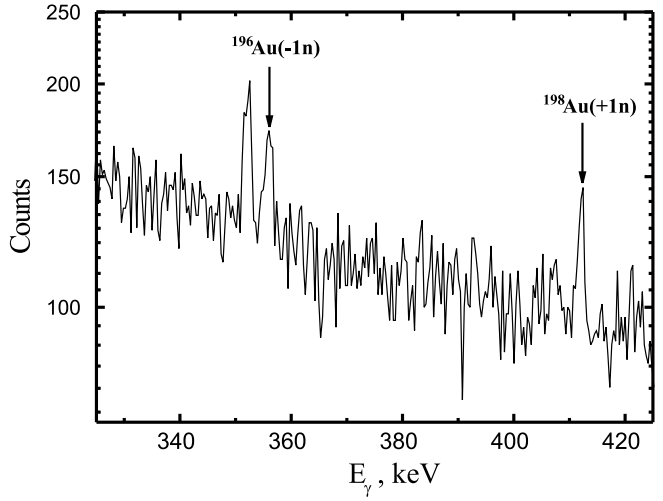

Fig. 4. Fragment of the γ-spectrum, obtained from measurement of the induced activity in the 5 μm Au foil irradiated with the ^{6}He beam at $\sim$ 7 MeV (Run 3). The γ-transition identification is shown next to the peaks.

The irradiation times in all four runs were much longer (sometimes several days) than the half-lives of most of the produced isotopes. For the correct calculation of the cross-sections, especially what concerned the short-lived nuclides, care was taken of their decay during the irradiation by means of constant monitoring of the beam current as a function of time. A spectrum of beam counting rate *versus* time was obtained and stored to a computer file. A relevant beam dose extracted from the data using 5 min time bins was taken for calculating the cross-sections of the individual isotopes. The plotted experimental cross-sections are the average of the values obtained in all γ-ray measurements of a particular residual nucleus for each individual target. The statistical errors for the cross-sections

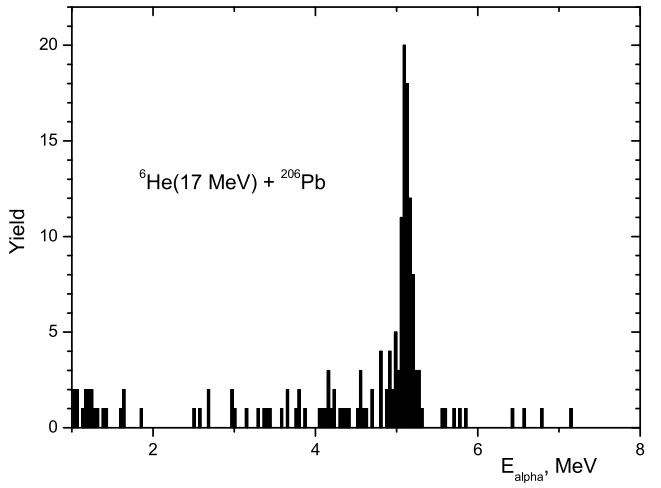

Fig. 5. Alpha-particle spectrum, obtained from measurement of the induced activity in the Pb foil, irradiated with the ^{6}He beam at $\sim$ 17 MeV.

have been obtained as the root mean square of the errors associated with all measurements (in turn, the error of each measurement includes the statistical error of the extracted peak area, the subtracted background, as well as the detector's efficiency errors).

We should note that in the range of the used ^{6}He incident energies on the Au targets, the recoil velocities of the evaporation residues and target-like products were small. Hence, the probability of some fraction of them to leave a target, pass to the next one and thus fall out of the data counting was assumed negligible. This holds true also for the ^{206}Pb targets, as the lead layer faced the beam.

The ^{206}Pb stack was measured using an α-spectrometer and the excitation function for the ^{206}Pb(^{6}He, 2n)^{210}Po reaction, viz. the formation of the compound nucleus ^{212}Po and its decay by emission of two neutrons, was obtained in the beam energy range 10–25.5 MeV (the Coulomb barrier for the given reaction is 21.5 MeV). The ^{210}Po isotope was identified by the α-particle energy (E_α = 5.3 MeV) and its half-life ($T_{1/2}$ = 138 d). The energy resolution of the α-spectrometer amounted to about 50 keV, and the total efficiency of registration of the α-particles was about 50%. A representative α-spectrum is shown in fig. 5.

3 Results and analysis

3.1 Fusion reactions

The cross-sections of the isotopes formed in the reaction $^{6}\mathrm{He} + {}^{197}\mathrm{Au} \rightarrow {}^{203-x}\mathrm{Tl}$, where x = 2–7, determined as described in the previous section, are shown in fig. 6 as a function of the bombarding energy (the excitation functions). The experimental cross-section values, obtained in the four runs (we should remind that the different runs are overlapping on the energy scale), have been plotted without any additional normalization.

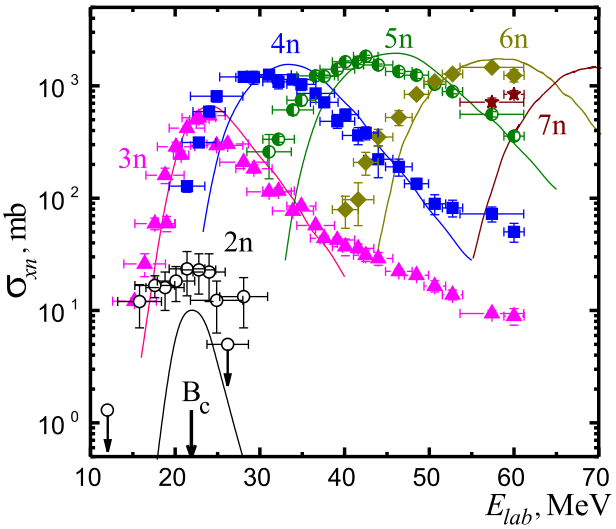

Fig. 6. (Colour online) Experimental excitation functions for the reaction $^{197}\mathrm{Au} + {}^{6}\mathrm{He} \rightarrow {}^{203-xn}\mathrm{Tl}$. The symbols denote: open circles, 2n; triangles, 3n; squares, 4n; semi-open circles, 5n; diamonds, 6n; stars, 7n evaporation channels; the curves are calculations with the "ALICE-MP" code [24] (see text and [26] for details). B_c is the Coulomb barrier.

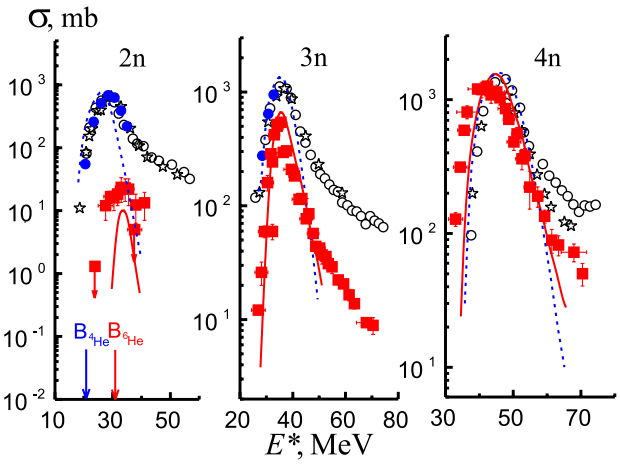

Fig. 7. (Colour online) Cross-sections for 2, 3 and 4n evaporation residues, obtained in the $^{197}\mathrm{Au}({}^{6}\mathrm{He}, x\mathrm{n})$ reaction (squares, present work), compared with data (filled and open circles, and stars) for the reaction $^{197}\mathrm{Au}({}^{4}\mathrm{He}, x\mathrm{n})$ from [27,28]. The solid and dashed curves are calculations with the "ALICE-MP" code [24] for the ^{6}He- and ^{4}He-induced reactions, respectively. The Coulomb barriers for the two reactions are indicated by arrows.

The analysis of the excitation functions for this reaction was performed using the fusion-evaporation code PACE4 [20] and the modified statistical model code "ALICE-MP" [24]. The calculated excitation functions in both methods are practically the same. Here, we briefly present the application of the "ALICE-MP" code. The calculations of the evaporation widths were based on the Weisskopf-Ewing formalism. In order to obtain the level density, the relations of the Fermi-gas model with allowance for shell effects in the level-density parameter were used [25]. In calculating reaction cross-sections associated with the evaporation of neutrons we considered a set of parameters, which determined the production cross-section for the compound nucleus and was connected with the geometric size of the nuclear part of the interaction potential (radius parameter r_0) and with its shape (diffuseness d of the potential and its depth V). The many calculations that have been performed to determine compound-nucleus production cross-sections and evaporation reaction channels for reactions with different particles (from ^{7}Li to ^{48}Ca) and targets (from Ca to Cf) have shown that, in most cases, we can use the same set of parameters, namely, $r_0 = 1.29\,\mathrm{fm}$, $V = -67\,\mathrm{MeV}$, and $d = 0.4\,\mathrm{fm}$. What concerns the critical angular momentum l_{cr}, that determines the number of partial waves leading to the formation of a compound nucleus, on the basis of rather general considerations concerning the mechanism of compound-nucleus formation, we assumed that l_{cr} has a square-root dependence on energy, as well as on the mass of the particle inducing the reaction. Varying the values of l_{cr} did not noticeably change the description of the data. We assumed that in the greater part of the energy range under consideration, the number of partial waves leading to compound-nucleus production is determined by the nuclear interaction potential. The values of the parameters given above have been used previously and proved to describe well the experimental data on the cross-sections of fission and xn evaporation channels in the reactions $^{4,6}\mathrm{He} + {}^{209}\mathrm{Bi}$ [26].

The calculations done with the ALICE-MP code for the given values of r_0, V and d are shown as solid curves in fig. 6. It can be seen that the experimental and calculated cross-sections at the maxima are in fair agreement in the case of the evaporation of 3–7 neutrons. Except that at energies to the right of the maxima, a retarded decrease in the cross-sections is present. Such high-energy "tails" have been formerly observed in α-particle induced reactions and have been explained as due to pre-equilibrium emission [27].

Direct analogy in the behaviour of the excitation functions of reactions induced by ^{6}He and ^{4}He can be demonstrated, if we compare the excitation functions of the two reactions $^{197}\mathrm{Au}({}^{6}\mathrm{He}, x\mathrm{n})$ and $^{197}\mathrm{Au}({}^{4}\mathrm{He}, x\mathrm{n})$ as a function of the excitation energy of the compound nucleus. Such a comparison is made in fig. 7 for the channels with evaporation of 2, 3 and 4 neutrons. The data for the $^{197}\mathrm{Au}({}^{6}\mathrm{He}, x\mathrm{n})$ reaction are from the present work, the values for $^{197}\mathrm{Au}({}^{4}\mathrm{He}, x\mathrm{n})$ are from [27,28]. The curves are calculations with the ALICE-MP code. As can be seen from the figure, the experimental points at the maxima and to some extent on the right slopes follow the calculated curves (except for the 2n data for ^{6}He). With increasing the excitation energy they deviate from the calculations (pre-equilibrium emission comes in), and the experimental cross-sections for the case of the incident ^{6}He fall off faster than in the case of ^{4}He. From the shown comparison, it follows that in the process of formation of a compound nucleus, at excitation energies corresponding to the maxima of the excitation functions, the α-particle

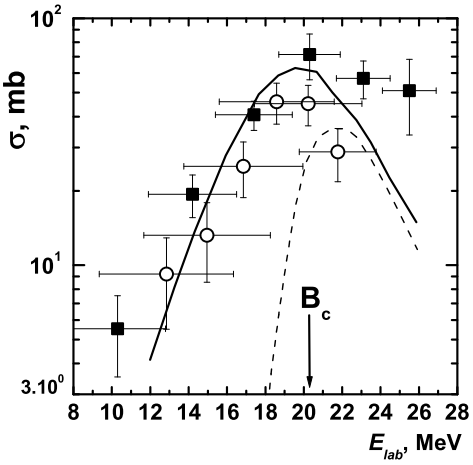

Fig. 8. Excitation function measured for the ^{206}Pb(^{6}He, 2n)^{210}Po reaction. The symbols are experimental cross-sections for the formation of ^{210}Po (open symbols are results from Run 1 [3,16], black —from Run 3). Dashed line: calculations within the framework of the statistical model; solid line: calculations using the two-step fusion model [29], taking into account the beam energy spread. B_c is the Coulomb barrier.

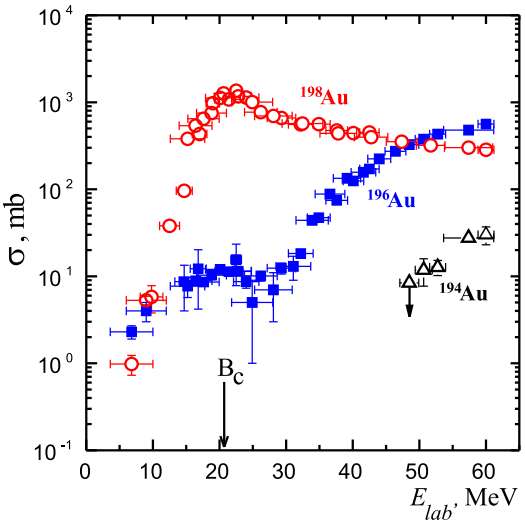

Fig. 9. (Colour online) Experimental excitation functions for the formation of the isotopes: ^{194}Au, triangles; ^{196}Au, squares and ^{198}Au, circles in the ^{197}Au + ^{6}He reaction. B_c is the Coulomb barrier.

core in ^{6}He behaves as a free ^{4}He nucleus. This could be expected due to the weak binding of the valence neutrons with the α-particle in ^{6}He. Obviously, at the higher energies in the 3n evaporation channel one pre-equilibrium neutron is emitted as a result of the interaction of the α-particle core with the target nucleus, while the other two are evaporation neutrons. In the 4n channel, the pre-equilibrium neutrons can be 1 or 2.

Contrary to the excitation functions for $x = 3$–7, the cross-sections for the 2n evaporation channel (the nucleus ^{201}Tl is formed) are significantly higher than the values calculated using the statistical model with the one-dimensional barrier between the interacting nuclei [24]. This may be connected with the fact that the reaction with total absorption of ^{6}He by the ^{197}Au target nucleus has a large positive Q-value, equal to +12.2 MeV. Thus, the position of the maximum of the excitation function for the evaporation of two neutrons is deeply below the barrier (the excitation energy of the formed compound nucleus at the Coulomb barrier is $\approx$ 33 MeV). Hence, the noticeable difference between the statistical model calculations and the experimental cross-sections could be due to sub-barrier enhancement.

We have observed quite a similar situation in the case of the interaction of ^{6}He with ^{206}Pb. The difference between the two reactions lies in the fact that in the ^{6}He + ^{206}Pb case, the Q-value is equal to +4.2 MeV. This, in turn, makes the 2n channel less "sub-barrier", and, consequently, leads to somewhat larger cross-section values.

The difference between experiment and calculations is particularly well seen in fig. 8, where the excitation function for the ^{206}Pb(^{6}He, 2n)^{210}Po reaction is shown. The cross-section for this reaction at the maximum, according to the statistical model calculations (the dashed line), should be small, because the maximum is situated at sub-barrier energies. However, as can be seen from the presented data, even at energies 7 MeV below the Coulomb barrier for the ^{206}Pb + ^{6}He reaction, the cross-section for formation of ^{210}Po, *i.e.* for the evaporation from the compound nucleus of two neutrons, is rather large and amounts to 10 mb. Thus, due to the observation of the reaction with the evaporation of two neutrons we could draw the conclusion that a considerable enhancement of the cross-section for the fusion of ^{6}He with ^{206}Pb exists at energies close to the barrier. In the same figure, the results of the calculations for the two-step fusion process are also presented [3,29]. In this model, it is assumed that a consecutive transfer of neutrons from the ^{6}He nucleus to the target nucleus takes place. At this, the excitation energy of the nuclear system increases by $E_{cm} + Q_{gg}$, a value which is quite higher than the Coulomb barrier and leads to the tunneling, at the latest stage, of the α-particle through the barrier. It can be seen that when the experimental spread in the incident energy has been taken into account, the observed enhancement in the cross-section of the ^{206}Pb + ^{6}He reaction is consistent with the calculation.

3.2 Transfer reactions

The measured excitation functions for the formation of the gold isotopes ^{194}Au, ^{196}Au and ^{198}Au in their ground states in the ^{6}He + ^{197}Au reaction are shown in fig. 9. We tried to explain the behaviour of the cross-sections from the point of view of kinematics and reaction dynamics.

The contribution of the transfer of charged particles and complete fusion to the formation of these isotopes is negligibly small. As shown by calculations within the statistical model, this probability amounts to less than

0.01 for the used energy range. As a result, mainly the neutron transfer contributes to the formation of the gold isotopes. Thus, the simplest ways in which target-like isotopes might be formed in the given reaction are: the isotopes ^{196}Au and ^{194}Au result after the removal of one and three neutrons from ^{197}Au, respectively, whereas ^{198}Au is formed after the pick-up by ^{197}Au of one neutron from ^{6}He. The isotope ^{199}Au was not observed, but we shall nevertheless comment on it in connection with the formation of the lighter isotopes. Besides, it should be noted that the xn separation energies in the target-like residues control the survivability of the given reaction products. To roughly estimate the minimum and maximum excitation energy in the heavy nucleus necessary for the emission of x-neutrons, we have used the prescription of ref. [30] with the values of nuclear masses and separation energies of one, two, etc. neutrons taken from [31].

The isotope ^{199}Au

The production of ^{199}Au involves a large reaction Q-value ($Q_{gg} = +13.12\,\mathrm{MeV}$), which means that there is kinematical mismatch, leading to a low cross-section. In fact, in our experiments, only an upper limit for the formation of the ^{199}Au isotope was determined, which gives evidence for the low probability of populating its ground state when ^{6}He interacts with ^{197}Au. Indeed, the transfer of two neutrons in this case takes place to particle-unbound states of ^{199}Au, which means that it immediately emits one or more neutrons.

The isotope ^{198}Au

As can be seen from fig. 9, close to the barrier the probability of producing the ^{198}Au isotope is rather large ($\sigma \sim 1.2\,\mathrm{b}$). At first consideration, this may be taken as direct evidence of large pure 1n transfer to the ^{197}Au target nucleus, followed by γ-transitions to its ground state. In fact, the reaction Q-value for the process of "^{6}He 1n-stripping" (or pick-up of one neutron by the ^{197}Au target nucleus) is $Q_{gg} = 4.65\,\mathrm{MeV}$, while the separation energy of one neutron from ^{198}Au is $B_{1n} = 6.51\,\mathrm{MeV}$; therefore, there is some probability for radiation transition to the ground state.

Another way of producing ^{198}Au is also possible, viz. in the transfer of two neutrons to ^{197}Au and de-excitation of the recoiling target-like nucleus ^{199}Au through the emission of one neutron: the channel of 1n-evaporation is open to produce ^{198}Au, since for ^{199}Au $Q_{gg} > B_{1n}(= 7.58\,\mathrm{MeV})$. At the same time, the probability of 3n transfer to ^{197}Au (producing ^{200}Au) with subsequent evaporation of two neutrons is expected to be small, due to the low possibility to pick up (in addition to the two valence neutrons of ^{6}He) one additional neutron from ^{4}He [28].

As is known that ^{197}Au has a large cross-section for pick-up of thermal neutrons, we studied the effect of background neutrons on the results. For this purpose, we placed a thick Au foil next to our stack. The γ-spectra measurements of this target showed that the contribution of the background neutron capture to produce ^{198}Au was insignificant.

As shown in fig. 9, the cross-section for the transfer of one neutron to ^{197}Au falls down to about 1 mb at $\sim 7\,\mathrm{MeV}$. The rather fast drop of the cross-section for the formation of ^{198}Au in the sub-barrier region can be considered also as due to the turning point of the entrance channel getting further when going away from the barrier and to the exponential dependence of the transfer form factor on the turning point radius.

The observed effect in our experimental data on ^{198}Au can be compared to the process of deuteron stripping. Indeed, such an effect is well known for (d, p) reactions, for which a significant increase of the cross-section, connected with the polarization of the weakly bound deuteron, is observed below the barrier (the so-called Oppenheimer-Phillips resonance [32]). In our case, this effect may be stronger because of the smaller neutron binding energy in ^{6}He compared to that for the deuteron and the larger repulsive forces of the α-particle compared to the proton. Additionally, it has been speculated that the observed enhanced ^{6}He total reaction cross-section is due to the quite probable dipole excitation, which occurs because the two halo neutrons are well separated from the charged core and the centers of charge and mass of the ^{6}He nucleus do not coincide [33]. For energies close to the Coulomb barrier dipole excitation can predominate as a result of the long-range Coulomb forces, which in turn lead to deformation and breakup of ^{6}He [34]. In both cases, neutrons can be transferred to the target nucleus.

In any case, the result obtained in the interaction of ^{6}He with ^{197}Au is consistent with the observed rather large one-neutron transfer in reactions with medium- and heavy-mass nuclei [11–14]. Together with this, the observation of enhanced sub-barrier fusion-fission cross-section in the $^{238}\mathrm{U} + {}^{6}\mathrm{He}$ reaction [9] can obviously be explained by fission after incomplete linear momentum transfer (*e.g.*, by the transfer of a neutron or inelastic excitation) to the highly fissile target.

The isotope ^{196}Au

The cross-section for pick-up from ^{197}Au of one neutron smoothly decreases in the vicinity of the Coulomb barrier, at a value of about 10 mb gets saturated, and after that falls down again until the value of the 1n transfer reaction threshold of $\sim 8.5\,\mathrm{MeV}$ is reached. This behaviour can be explained by different mechanisms of formation of the ^{196}Au isotope ($-$1n channel). At energies well above the Coulomb barrier, it seems that a predominantly knock-out of a neutron from the target occurs. At energies close to and below the Coulomb barrier, several contributions to the formation of ^{196}Au are possible. One is due to the evaporation of one neutron after an inelastic process on ^{197}Au (excited ^{197}Au* nuclei are produced). ^{196}Au can be produced after the evaporation of three neutrons from ^{199}Au, if the latter were excited to $E^{*} \approx 27$–$36\,\mathrm{MeV}$. Additionally, the recoil nucleus ^{198}Au, produced in the 1n

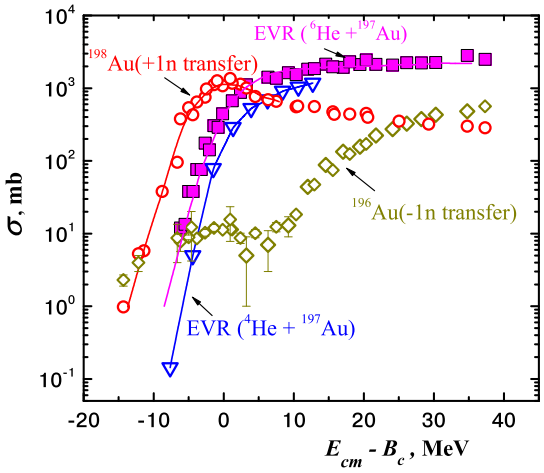

Fig. 10. (Colour online) Experimental cross-sections for complete fusion (squares), for formation of ^{196}Au (diamonds) and ^{198}Au (circles) in the reaction ^{6}He + ^{197}Au (present work), and for complete fusion (inverted triangles) in the ^{4}He + ^{197}Au reaction [28] as a function of the difference between the center-of-mass energy and the Coulomb barrier ($E_{cm} - B_c$). The curves are drawn to guide the eye.

transfer channel, can be excited to $E^* \approx 18$–32 MeV so that it can decay to ^{196}Au by the emission of two neutrons. These processes can explain, at least partially, the flat shape of the excitation function, observed in the region $E_{lab} \approx 12$–28 MeV.

The isotopes ^{194}Au and ^{195}Au

The isotope ^{195}Au has characteristics that are not convenient for its detection. It has a relatively long (186.09 days) half-life and its most intensive γ-ray is in the region of energies, where we observed significant background. The isotope ^{194}Au was observed in the beam energy range ($\sim$ 50–60 MeV) and as is shown in fig. 9, its formation cross-section amounts to $\sim$ 30 mb, but quickly decreases with energy and at 48.5 MeV only an upper limit of 8.4 mb was measured.

The cross sections for the fusion reaction channel (denoted as EVR) and for the transfer channels (conditionally called "+1n transfer" and "−1n transfer") in the interaction of ^{6}He with ^{197}Au are presented in fig. 10 as a function of the difference between the center-of-mass energy of the incident particle and the reaction Coulomb barrier, $E_{cm} - B_c$. The excitation function for the fusion of ^{4}He with ^{197}Au is also shown for comparison. One can see the increase in the cross-section for the ^{6}He + ^{197}Au fusion reaction in the sub-barrier region compared to the case of ^{4}He, and also the rather strong increase of the formation cross-section of ^{198}Au.

4 Conclusions

In the present paper, we have presented results on the measurements of the excitation functions for fusion and transfer products in ^{6}He-induced reactions on ^{197}Au and ^{206}Pb in a wide energy range including deep sub-barrier energies. The experiments were performed at the accelerator complex DRIBs in Dubna, the ^{6}He beam intensity reaching 2×10^{7} pps at 10 AMeV.

The following conclusions can be drawn. The data on fusion reactions, followed by the evaporation of two neutrons (^{206}Pb + ^{6}He and ^{197}Au + ^{6}He) at energies close to the Coulomb barrier differ from predictions within the framework of the statistical model for compound-nuclei decay. The observed enhancement in the ^{206}Pb + ^{6}He reaction is consistent with calculation within the model of "sequential fusion" [29]. The reaction of the transfer of one neutron from ^{6}He to the ^{197}Au target nucleus at deep sub-barrier energies ($B_{cm} - E_{cm} \leq 15$ MeV) takes place with relatively high probability.

Finally, the authors would like to express their gratitude to the accelerator staff for the great effort to put into operation the accelerator complex DRIBs and to obtain the ^{6}He beam. We are also indebted to M.G. Itkis and S.N. Dmitriev for their support, and to V.I. Zagrebaev for making available his calculations of the fusion reaction cross-sections and for fruitful discussions. Thanks are due also to D.N. Rassadov, S.V. Shishkin and J. Adam for their help during the measurements. The present investigation was carried out with the support of RFBR by grant No. 04-02-17372, grant Russia-Flandria 05-02-19813 MF, as well as by grants from Bulgaria, the Czech Republic and Poland in the frame of their collaboration with JINR.

References

1. M. Beckerman, Rep. Prog. Phys. **51**, 1047 (1988) and references therein.
2. R.A. Broglia, C.H. Dasso, S. Landowne, A. Winther, Phys. Rev. C **27**, 2433R (1983) and references therein.
3. Yu.E. Penionzhkevich, V.I. Zagrebaev, S.M. Lukyanov, R. Kalpakchieva, Phys. Rev. Lett. **96**, 162 (2003).
4. S. Saha, Y.K. Agarwal, Nucl. Phys. A **601**, 251 (1996).
5. J.F. Liang, C. Signorini, Int. J. Mod. Phys. E **14**, 1121 (2005).
6. L.F. Canto, P.R.S. Gomes, R. Donangelo, M.S. Hussein, Phys. Rep. **424**, 1 (2006).
7. Yu.E. Penionzhkevich, Nucl. Phys. A **588**, 259c (1995); Yu.E. Penionzhkevich, Yu.A. Muzychka, S.M. Lukyanov, R. Kalpakchieva, N.K. Skobelev, V.P. Perelygin, Z. Dlouhy, Eur. Phys. J. A **13**, 123 (2002).
8. J.J. Kolata, V. Guimaraes, D. Peterson, P. Santi, R. White-Stevens, P.A. DeYoung, G.F. Peaslee, B. Hughey, B. Atalla, M. Kern, P.L. Jolivette, J.A. Zimmerman, M.Y. Lee, F.D. Becchetti, E.F. Aguilera, E. Martinez-Quiroz, J.D. Hinnefeld, Phys. Rev. Lett. **81**, 4580 (1998).
9. M. Trotta, J.L. Sida, N. Alamanos, A. Andreyev, F. Auger, D.L. Balabanski, C. Borcea, N. Coulier, A. Drouart, D.J.C. Durand, G. Georgiev, A. Gillibert, J.D. Hinnefeld, M. Huyse, C. Jouanne, V. Lapoux, A. Lepine, A. Lumbroso, F. Marie, A. Musumarra, G. Neyens, S. Ottini, R. Raabe, S. Ternier, P. Van Duppen, K. Vyvey, C. Volant, R. Wolski, Phys. Rev. Lett. **84**, 2342 (2000).

10. R. Raabe, J.L. Sida, J.L. Charvet, N. Alamanos, C. Angulo, J.M. Casandjian, S. Courtin, A. Drouart, D.J.C. Durand, P. Figuera, A. Gillibert, S. Heinrich, C. Jouanne, V. Lapoux, A. Lepine-Szily, A. Musumarra, L. Nalpas, D. Pierroutsakou, M. Romoli, K. Rusek, M. Trotta, Nature **431**, 823 (2004).
11. A. Di Pietro, P. Figuera, F. Amorini, C. Angulo, G. Cardella, S. Cherubini, T. Davinson, D. Leanza, J. Lu, H. Mahmud, M. Milin, A. Musumarra, A. Ninane, M. Papa, M.G. Pellegriti, R. Raabe, F. Rizzo, C. Ruiz, A.C. Shotter, N. Soic, S. Tudisco, L. Weissman, Phys. Rev. C **69**, 044613 (2004).
12. A. Navin, V. Tripathi, Y. Blumenfeld, V. Nanal, C. Simenel, J.M. Casandjian, G. de France, R. Raabe, D. Bazin, A. Chatterjee, M. Dasgupta, S. Kailas, R.C. Lemmon, K. Mahata, R.G. Pillay, E.C. Pollacco, K. Ramachandran, M. Rejmund, A. Shrivastava, J.L. Sida, E. Tryggestad, Phys. Rev. C **70**, 044601 (2004).
13. E.F. Aguilera, J.J. Kolata, F.M. Nunes, F.D. Becchetti, P.A. DeYoung, M. Goupell, V. Guimaraes, B. Hughey, M.Y. Lee, D. Lizcano, E. Martinez-Quiroz, A. Nowlin, T.W. O'Donnell, G.F. Peaslee, D. Peterson, P. Santi, R. White-Stevens, Phys. Rev. Lett. **84**, 5058 (2000); E.F. Aguilera, J.J. Kolata, F.D. Becchetti, P.A. DeYoung, J.D. Hinnefeld, A. Horvath, L.O. Lamm, Hye-Young Lee, D. Lizcano, E. Martinez-Quiroz, P. Mohr, T.W. O'Donnell, D.A. Roberts, G. Rogachev, Phys. Rev. C **63**, 061603R (2001); J.J. Kolata, Eur. Phys. J. A **13**, 117 (2002).
14. J.P. Bychowski, P.A. DeYoung, B.B. Hilldore, J.D. Hinnefeld, A. Vida, F.D. Becchetti, J. Lupton, T.W. O'Donnell, J.J. Kolata, G. Rogachev, M. Hencheck, Phys. Lett. B **596**, 26 (2004).
15. Yu.Ts. Oganessian, G.G. Gulbekian, in *Proceedings of the International Conference Nuclear Shells - 50 Years*, edited by Yu.Ts. Oganessian, R. Kalpakchieva (World Scientific, Singapore, 2000) p. 61.
16. Yu.E. Penionzhkevich, R.A. Astabatyan, N.A. Demekhina, Z. Dlouhy, R. Kalpakchieva, A.A. Kulko, S.P. Lobastov, S.M. Lukyanov, E.R. Markaryan, V.A. Maslov, Yu.A. Muzychka, Yu.Ts. Oganessian, D.N. Rassadov, N.K. Skobelev, Yu.G. Sobolev, V.Yu. Ugryumov, J. Vincour, T. Zholdybaev, Phys. Part. Nuclei, Lett. **3**, no. 6, 38 (2006).
17. V.D. Kuznetsov, G.V. Mishinsky, V.I. Arbuzov, D.V. Kamanin, S.V. Mitrofanov, V.I. Zhemenik, in *Scientific report FLNR 2001-2002*, edited by A.G. Popeko (JINR, Dubna, 2003) pp. 223, 224.
18. R.A. Astabatyan, R.L. Kavalov, A. Kugler, I.V. Kuznetsov, V.F. Kushniruk, S.P. Lobastov, S.M. Lukyanov, E.R. Markaryan, V.A. Maslov, L. Mikhailov, Yu.E. Penionzhkevich, N.O. Poroshin, N.K. Skobelev, V.I. Smirnov, Yu.G. Sobolev, V.Yu. Ugryumov, Bull. Russ. Acad. Sci. Phys. **67**, 756 (2003).
19. N.K. Skobelev, R. Kalpakchieva, R.A. Astabatyan, J. Vincour, A.A. Kulko, S.P. Lobastov, S.M. Lukyanov, E.R. Markaryan, V.A. Maslov, Yu.E. Penionzhkevich, Yu.G. Sobolev, V.Yu. Ugryumov, Nucl. Instrum. Methods B **227**, 471 (2005).
20. `http://dnr080.jinr.ru/lise/`; `http://groups.nscl.msu.edu/lise/`.
21. J. Frana, Radioanal. Nucl. Chem. **257**, 583 (2003).
22. `http://nucleardata.nuclear.lu.se/NuclearData/toi/`.
23. Z.G. Gritchenko, T.P. Makarova, Yu.Ts. Oganessian, Yu.E. Penionzhkevich, A.V. Stepanov *et al.*, Phys. At. Nuclei **10**, 929 (1969) (in Russian).
24. Yu.A. Muzychka, B.I. Pustylnik, Phys. At. Nuclei **45**, 90 (1987).
25. A.V. Ignatyuk, G.N. Smirenkin, A.S. Tishin, Yad. Fiz. **21**, 485 (1975) [Sov. J. Nucl. Phys. **21**, 255 (1975)].
26. Yu.E. Penionzhkevich, Yu.A. Muzychka, S.M. Lukyanov, R. Kalpakchieva, N.K. Skobelev, V.P. Perelygin, Yu.G. Sobolev, L.V. Mikhailov, V.Yu. Ugryumov, J. Vincour, Z. Dlouhy, L. Kostov, Ya. Mrazek, N.O. Poroshin, Phys. At. Nuclei **65**, no. 9, 1563 (2002).
27. F.M. Lanzafame, M. Blann, Nucl. Phys. A **142**, 545 (1970); H.E. Kurz, E.W. Jasper, K. Fischer, F. Hermes, Nucl. Phys. A **168**, 129 (1971).
28. A.A. Kulko, N.A. Demekhina, R. Kalpakchieva, Yu.A. Muzychka, Yu.E. Penionzhkevich, D.N. Rassadov, N.K. Skobelev, D.A. Testov, Phys. At. Nuclei **70**, no. 4, 1 (2007); also `http://www.jinr.ru/publish/Preprints/2006/014(P7-2006-14).pdf`, Dubna 2006 (in Russian).
29. V.I. Zagrebaev, Phys. Rev. C **67**, 061601(R) (2003); Prog. Theor. Phys. Suppl. **154**, 122 (2004).
30. R. Bimbot, D. Gardes, M.F. Rivet *et al.*, Nucl. Phys. A **189**, 193 (1972).
31. G. Audi, A.H. Wapstra, C. Thibault, Nucl. Phys. A **729**, 337 (2003).
32. J.R. Oppenheimer, M. Phillips, Phys. Rev. **48**, 500 (1935).
33. K. Rusek, N. Keeley, K.W. Kemper, R. Raabe, Phys. Rev. C **67**, 041604(R) (2003); N. Keeley, J.M. Cook, K.W. Kemper, B.T. Roeder, W.D. Weintraub, F. Marechal, K. Rusek, Phys. Rev. C **68**, 054601 (2003).
34. C.H. Dasso, J.L. Guisado, S.M. Lenzi, A. Vitturi, Nucl. Phys. A **597**, 473 (1996).